The Response of a Coupled Ocean–Atmosphere General Circulation Model to Wind Bursts

M. LATIF, J. BIERCAMP AND H. VON STORCH

Max-Planck-Institut für Meteorologie, Hamburg, F.R.G.

(Manuscript received 27 April 1987, in final form 28 September 1987)

ABSTRACT

A coupled ocean–atmosphere general circulation model has been developed for TOGA related problems. The coupled model consists of an ocean model of the tropical Pacific and a global low-order spectral atmosphere model. The two models interact via wind stress and sea surface temperature. In order to avoid a climate drift within the coupled model, a flux correction method is applied.

Experiments were performed by introducing a westerly wind stress burst over the western equatorial Pacific for one month. Thereafter, the wind burst is turned off and the response of the coupled model to the initial disturbance is investigated. The results are compared with the response of the ocean model run with the same disturbance in an uncoupled mode.

It is shown that the coupling leads to a significant increase of the duration of anomalous conditions in the ocean. SST anomalies persist for about 12 months in the coupled run, while they have already disappeared after 4 months in the uncoupled case. The increase in persistence is due to the feedback of the atmosphere, which responds with an eastward shift of the ascending branch of the Walker Circulation.

In a second experiment with the coupled model the initial disturbance was introduced within another season. The results show no basic differences to the results of the first experiment.

An interesting result of the coupled model runs is the occurrence of spontaneous westerly wind bursts over the western Pacific, which developed by internal dynamics. Location and duration of these spontaneous wind bursts show some correspondence with the time–space structure of observed westerly wind stress episodes over the western Pacific.

1. Introduction

The dominant signal of the climate system in the tropics on the time scale of several months to a few years is the so called El Niño/Southern Oscillation phenomenon (ENSO). During ENSO periods serious anomalies of different oceanic and atmospheric variables such as sea surface temperature (SST), rainfall and sea level pressure are observed. Reviews on the ENSO phenomenon can be found for instance in Gill and Rasmusson (1983), Cane (1983) or Rasmusson and Wallace (1983).

General circulation models (GCM) of both the atmosphere and of the ocean have been used during the last few years to investigate low frequency changes of the climate system in the tropics associated with ENSO events and their impact on the atmospheric circulation in midlatitudes. The success of these models in reproducing observed circulation anomalies is due to the fact that low frequency changes of the tropical oceans and atmospheres are caused primarily by low frequency changes of the appropriate boundary conditions. Until now most of the studies have been performed with models of one component of the climate system run in an uncoupled mode, the other component being represented by prescribing boundary conditions from observations.

For example Lau (1985) demonstrated that over a 15-year period the tropical atmospheric circulation over the Pacific Ocean can be simulated realistically with respect to interannual variability, if actual SST data are used to force the GCM. In a repeat experiment started with other initial conditions the low frequency response was almost unaltered, showing the stability of the boundary forced response. Fennessy et al. (1985) studied the evolution of the 1982/83 ENSO event in the atmosphere. The temporal and spatial structure of observed changes, such as rainfall or low level wind anomalies were reproduced realistically by their atmospheric GCM. In general, atmospheric GCMs seem to be capable of simulating observed low frequency changes of tropical atmospheres.

The complementary problem has been investigated using oceanic GCMs, wind stress and surface heat flux being prescribed at the upper boundary. The ocean models show also realistic variations, if observed wind stress fields are used as forcing. For example, Philander and Seigel (1985) simulated the 1982/83 ENSO event in the ocean and succeeded in reproducing basic aspects of observed temperature and current changes. Latif

Corresponding author address: Dr. Mojib Latif, Max-Planck-Institut fur Meteorologie, Bundesstr. 55, D-2000 Hamburg 13, F.R.G.

(1987) ran an oceanic GCM for more than two decades. The calculated sea level and SST anomalies showed a reasonable correspondence with the observed anomalies during the period of integration.

Both the atmospheric and the oceanic modeling branches imply that it should be possible to develop coupled ocean–atmosphere models which will succeed in simulating realistic low frequency changes of the climate system in the tropics. Until now only a few coupled models have been developed. The first GCM-type coupled model was run by Gates et al. (1985). In this study the coupled system showed a serious climate drift. In particular, the trade wind system over the tropical Pacific Ocean disappeared quickly. This led to a SST distribution without the typical zonal gradient along the equator. The coupled model stayed in this state and showed no evidence of an ENSO type variability. Other coupled models were developed by Bryan and Manabe (1985) and by Washington et al. (1985), but these models were not designed primarily for ENSO related problems. Recently, Zebiak (1984) constructed a simple regional coupled model for the purpose of investigating ENSO problems. In this model the climatological mean state is prescribed, so that the model predicts anomalies around this state. The coupled model shows a quite realistic behaviour with respect to interannual variability. In particular, SST anomalies undergo the typical irregular variations. This model was also used for the purpose of prediction (Cane et al., 1986). In most cases the model was successful in predicting the observed evolution of equatorial SST anomalies.

According to Philander (1986) there are two extremes for the explanation of the oscillatory behavior of ENSO. One idea is based on the propagation of waves in the ocean and their reflexion at meridional boundaries. Small disturbances on the equator can be amplified by unstable air–sea interactions (Philander et al., 1984). Planetary waves are radiated from the instability region, propagating to the west in higher latitudes. By reflexion at the western boundary an equatorial disturbance can be generated, which propagates eastward and which can grow again by unstable air–sea interactions. Thus, the memory of the coupled system lies entirely in the ocean. This scenario is applicable for the model of Schopf and Suarez (1985), who coupled a two layer oceanic GCM to a two layer atmospheric model.

Another way of explaining the irregular behavior of ENSO is to attribute their origin to atmospheric disturbances. The atmosphere contains a lot of noise, one example of which are the "30–60 day" Oscillations. These disturbances can also be amplified by unstable air–sea interactions and can result finally in ENSO episodes, if the ocean matches certain conditions. Such an explanation was suggested by Lau (1985), who developed a simple nonlinear oscillator-type model. The same mechanism was suggested by Wyrtki (1985), who regards ENSO cycles as a combination of atmospheric randomness and a deterministic ocean. Wyrtki postulated as a necessary oceanic condition that the western Pacific has accumulated a certain amount of warm water, which is released to higher latitudes during ENSO events. Models based on this idea assume that ENSO events are solely triggered by the atmosphere, but that the ocean must be preconditioned. Common to both explanations is the assumption that unstable air–sea interactions are possible. Therefore a coupled ocean–atmosphere model is needed for the study of complete ENSO cycles.

In this paper we present such a coupled ocean–atmosphere model, which has been developed for ENSO related problems. It uses general circulation models of both, the equatorial Pacific Ocean and the global atmosphere. We make use of a flux correction method at the interface of the two models. This method avoids a climate drift of the coupled system without violating its dynamics for variability studies.

The coupled model belongs to the class of models in which ENSO is assumed to be initiated by atmospheric disturbances. The experiments described here address the instability behavior of the coupled model and its dependence on the seasonal cycle. We investigate the importance of coupled feedbacks in our sophisticated model, which were shown to play a crucial role in more simple models of air–sea interaction (e.g., Hirst, 1985). In the experiments an anomaly of surface wind stress was introduced initially over the western Pacific Ocean. The response of the coupled model to this initial disturbance was then investigated and compared with the results of the unperturbed runs, and with the results of the ocean model run in an uncoupled mode.

The paper is organized as follows. The coupled model is described in chapter two. In chapter three we present the results, which are summarized and discussed in chapter four.

2. Model

The coupled model consists of a regional ocean model of the tropical Pacific and a global atmosphere model. The ocean model is basically the model described in Latif (1987) and is a primitive equation model which calculates the three dimensional current field, sea level and sea surface temperature. The model domain (Fig. 1) is the tropical Pacific Ocean from 30°S to 30°N and from 130°E to 70°W. The model includes real coastlines but no bottom topography, so that the ocean floor is at a constant depth of 4000 m. The zonal resolution is constant with a grid distance of 670 km. The meridional resolution is variable, increasing from 50 km around the equator to about 400 km at the northern and southern boundary. We use 13 levels in the vertical direction, most of them being placed within the upper 300 m.

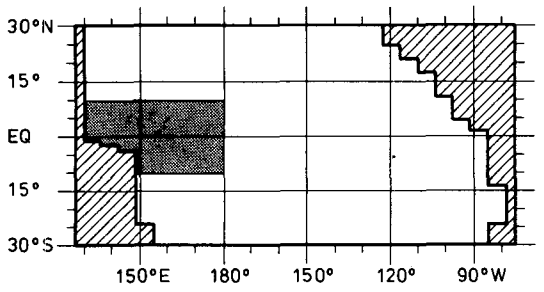

FIG. 1. Domain of the ocean model. The shaded area indicates the region of anomalous forcing.

The atmosphere model is the T-21 version of the ECMWF model. The model, described in detail by Duemenil and Schlese (1987), is a global low order spectral model with a triangular truncation at wavenumber 21 and 16 irregularly spaced levels in the vertical. The model includes standard physics.

The coupling of the two models occurs in both directions (Fig. 5). The atmosphere model is driven by the SST calculated by the ocean model. Outside the domain of the ocean model the SST varies seasonally and it is taken from observations. The resulting vertical fluxes of momentum, heat, and moisture are determined by the atmosphere model itself.

The ocean model is forced by the wind stress of the atmosphere model and a noninteractive heat flux Q according to Haney (1971):

$$Q = \alpha(T_F - T),$$

where T is the temperature of the ocean at 10 m depth. The "forcing temperature" T_F is assumed to be two degrees higher than the observed climatological air temperature at 2 m height, the coefficient α has a value of approximately 17 W m^{-2} K^{-1}, corresponding to a relaxation time of about 30 days for the upper layer of 10 m thickness. With this noninteractive heat flux the coupled system is heavily damped. It will be shown later that the coupled model still has enough freedom to respond to an externally introduced atmospheric disturbance via anomalous heating of the atmosphere and subsequently changed circulation.

The interactive quantities, SST and wind stress are corrected by constant offset quantities (Fig. 5), because the models run in an uncoupled mode show already significant deviations from climatology. This fact is exemplified by Figs. 2, 3 and 4. As can be seen, the pattern of SST is simulated reasonably well by the ocean model (Fig. 2a). However, due to an overestimation of equatorial upwelling in the ocean model, we find large SST errors in the equatorial zone, reaching values of more than 4°C (Fig. 2c).

The errors in wind stress are shown in Figs. 3 and 4, and are discussed in more detail in Biercamp and von Storch (1987). The model climatology was calculated from a ten-year simulation using climatological seasonal forcing (Kirk et al., 1987). As can be seen, the pattern of wind stress is simulated realistically by the atmosphere model. Nevertheless, the amplitudes are much too weak. The simulated zonal wind stress component for example (Fig. 3a) shows the two maximum regions corresponding to the northeast and southeast trades. The strength, however, is only about half of the observed values (Fig. 3b). This is clearly seen in the difference map (Fig. 3c), which shows that the errors are of the same order of magnitude as the simulation itself. The errors are even worse for the meridional wind stress component (Fig. 4). The intertropical convergence zone as well as the South Pacific convergence zone are only marginally present in the model simulation (Fig. 4a). The model underestimates not only the strength of the meridional wind stress component but also its strong meridional gradient within the innertropical convergence zone. Because of the weak model fields the difference map between observation and simulation (Fig. 4c) looks almost like the observed map. As a result of these significant model errors a coupled model built with the two components described above would presumably enter into a climate drift and move into a new climate state which would

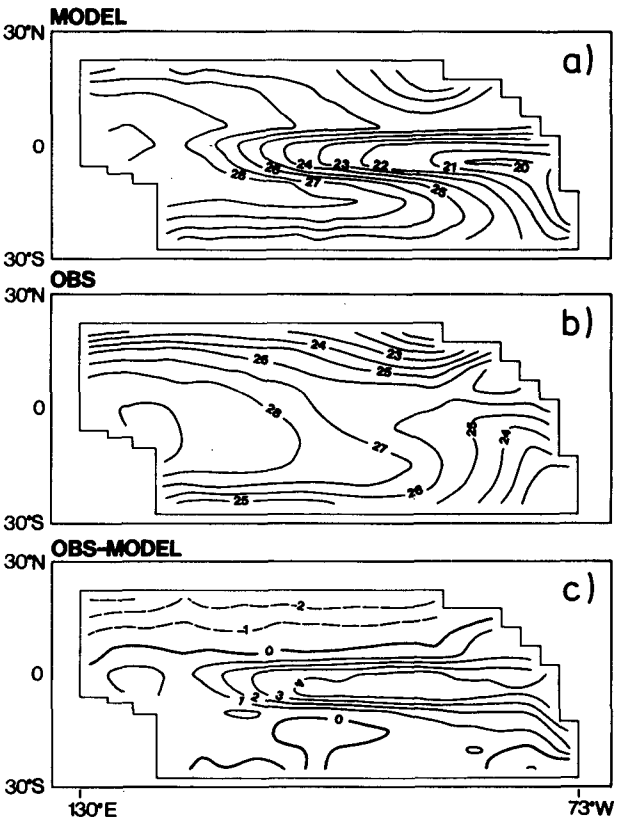

FIG. 2. Simulation of SST for January, (a) uncoupled model simulation, (b) observed climatology (from Esbensen and Kushnir, 1981) and (c) model error.

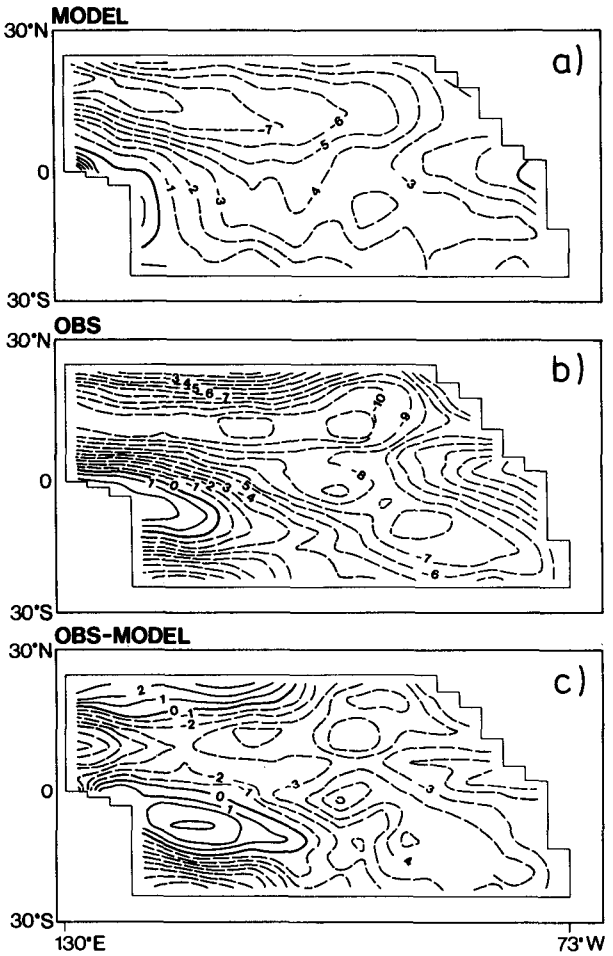

FIG. 3. Simulation of zonal wind stress, (a) uncoupled model simulation, (b) observed climatology and (c) model error. The observed values are calculated from the dataset of Goldenberg and O'Brien (1981), contour interval 10^{-2} N m^{-2}.

be far away from the present climate state. An appropriate method to avoid climate drift in coupled models has been worked out by Sausen et al. (1987). They suggest a flux correction method, in which the interactive fluxes are corrected by constant quantities which are determined in advance from the uncoupled control runs. By means of such a correction method artificial sources or sinks of fluxes are introduced at the interface of the models and the continuity of fluxes across the interface is violated. However, the main point of this flux correction method is that the correction is constant and does not depend on the current state of the coupled system. Thus, the dynamics of the coupled model is not altered significantly in variability studies by the flux correction method. We apply in this paper a slightly modified version of this more general concept and correct for sea surface temperature and wind stress (Fig. 5):

$$T = T_O^c + \Delta T$$

$$\vec{\tau} = \vec{\tau}_A^c + \Delta\vec{\tau};$$

$$\Delta T = T_{\text{obs}} - T_O^u, \quad \Delta\vec{\tau} = \vec{\tau}_{\text{obs}} - \vec{\tau}_A^u.$$

Here the subscript O refers to ocean quantities, the subscript A to atmospheric values and the subscript "obs" denotes observed quantities. The superscripts c and u refer to quantities from the coupled run and from the uncoupled run, respectively. The temperature T is used as boundary temperature for the atmosphere, while T_O^c is the temperature of the uppermost level of the ocean model within the coupled system. Similarly, the stress $\vec{\tau}$ drives the ocean model, while the atmospheric model experiences the stress $\vec{\tau}_A^c$. The corrections ΔT and $\Delta\vec{\tau}$ are exactly the model errors, which are shown for January in Figs. 2, 3 and 4. We take into account a seasonal variation of the correction terms, but as was already pointed out, the corrections ΔT and $\Delta\vec{\tau}$ do not depend on the state of the coupled model. By means of this correction technique we hope to pre-

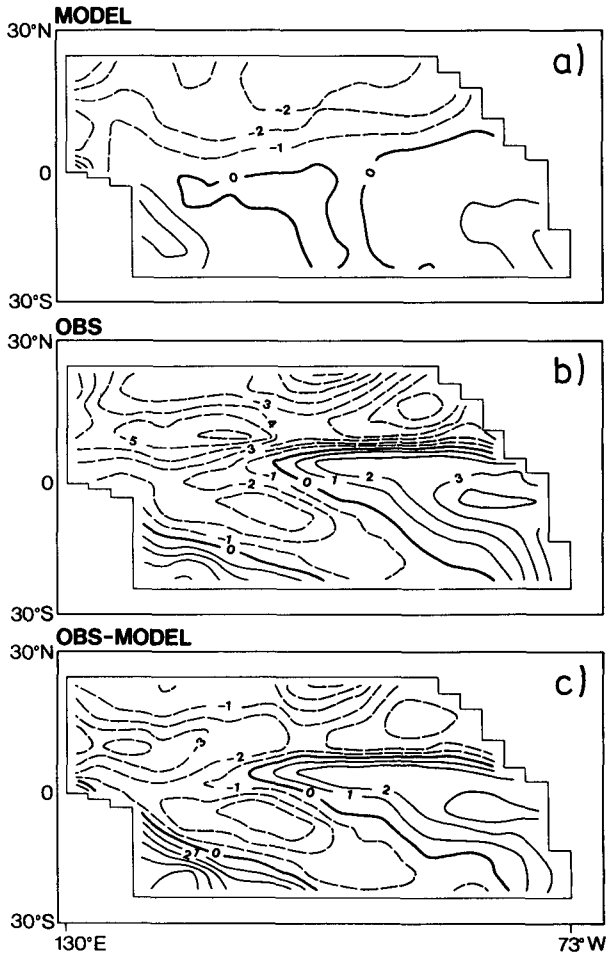

FIG. 4. As in Fig. 3, but for the meridional wind stress component.

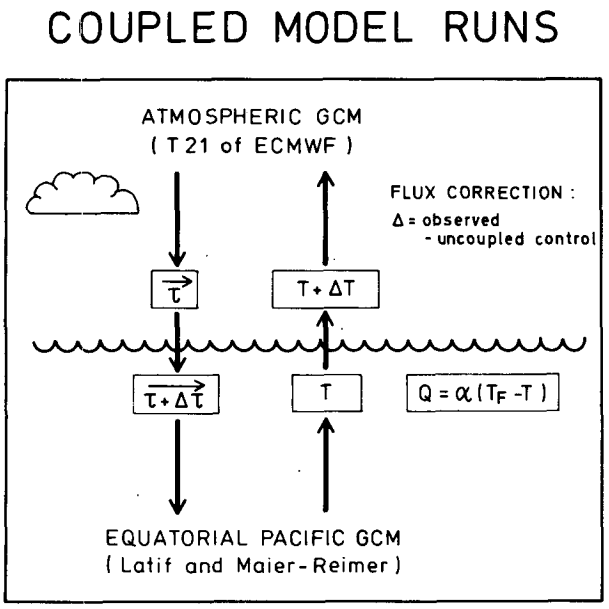

FIG. 5. Technique of coupling.

scribe an equilibrium state of the coupled system. This state, however, could be unstable, but as will be shown later, the coupled model does not drift into another climate state.

3. Results

a. Description of experiments

In this chapter we describe a set of five experiments. Two experiments were performed with the ocean model, run in an uncoupled mode, while the other three experiments were performed with the coupled model. The performed experiments are listed in Table 1.

In a first experiment ("uncoupled control" run) the ocean model was forced with seasonally varying forcing until it reached an almost cyclostationary state after 3 years. The wind forcing was calculated from the dataset of Goldenberg and O'Brien (1981). In a second experiment ("uncoupled anomaly run") we prescribed an anomalous wind stress in the western Pacific from 10°S to 10°N and from 130°E to 180° during January of one additional cycle. For this particular month the total surface wind stress in the region of anomalous forcing (shaded area in Fig. 1) is assumed to be purely zonal with a value of 0.18 N m^{-2}, corresponding to a zonal surface wind of 10 m s^{-1}. (At this time the climatological zonal wind stress at the dateline, for instance, is directed westward, so that the effective zonal wind stress anomaly is even larger there.) Thereafter the calculation was continued using the same forcing as in the uncoupled control run. Anomalies are determined by subtracting the results of the two uncoupled runs from each other. In experiments 3 and 4 we repeated experiments 1 and 2 with the coupled model. Experiment 5 differs from experiment 4 only in that the January initial conditions are replaced by July initial conditions.

TABLE 1. List of experiments.

Experiment	Model	Initial burst
1. Uncoupled control	Ocean GCM	none
2. Uncoupled anomaly	Ocean GCM	January
3. Coupled control	Coupled GCM	none
4. Coupled anomaly	Coupled GCM	January
5. Coupled anomaly	Coupled GCM	July

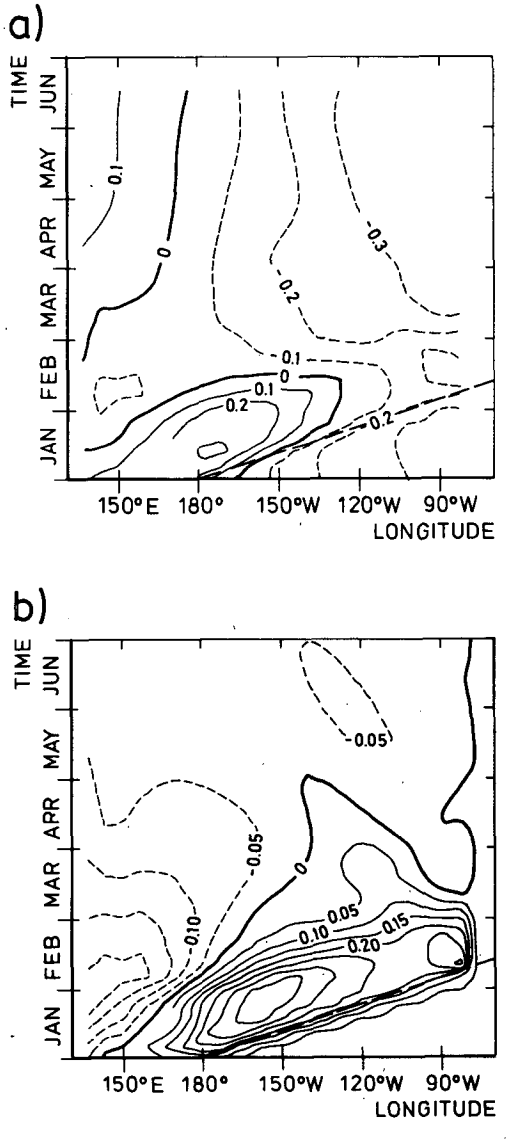

FIG. 6. Evolution of sea level along the equator for the uncoupled anomaly run, (a) full signal (contour interval 0.1 m) and (b) anomalies (contour interval 0.05 m). The dashed straight line shows the path of the first mode Kelvin wave.

b. Uncoupled runs

Figures 6 and 7 show the evolution of sea level and SST in the uncoupled anomaly run together with their anomalies. The sea level response (Fig. 6) along the equator is very similar to the response one would expect from linear wave theory (see McCreary, 1976). Baroclinic Kelvin waves are excited by the abrupt changes of the zonal wind stress in the western Pacific. Sea level rises very quickly to the east of the region of anomalous forcing. The sea level signal propagates eastward with a speed of about 2.8 m s^{-1}, which corresponds to the phase speed of the first baroclinic mode, as indicated by the dashed straight line in Figs. 6a and 6b. At the eastern boundary the ocean model shows a second maximum in sea level, which is due to a first mode planetary wave and which adds to the sea level. This planetary wave is created by reflection of the incident Kelvin wave at the eastern boundary and travels westward with one third of the Kelvin wave speed. When the disturbance of surface wind stress is suddenly turned off after one month, the system rapidly relaxes back to normal. Kelvin waves now lower sea level to the east of the forcing region. After about 4 months sea level anomalies are within the range of 5 cm (Fig. 6b) and the isohypses in Fig. 6a do not show any significant tilts.

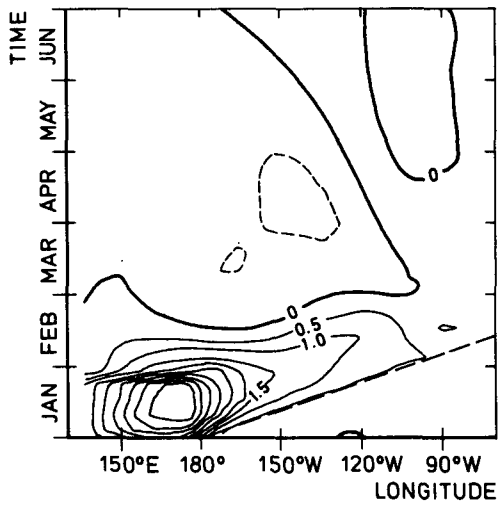

FIG. 8. Evolution of zonal surface current anomalies along the equator for the uncoupled anomaly run, contour interval 0.5 m s^{-1}.

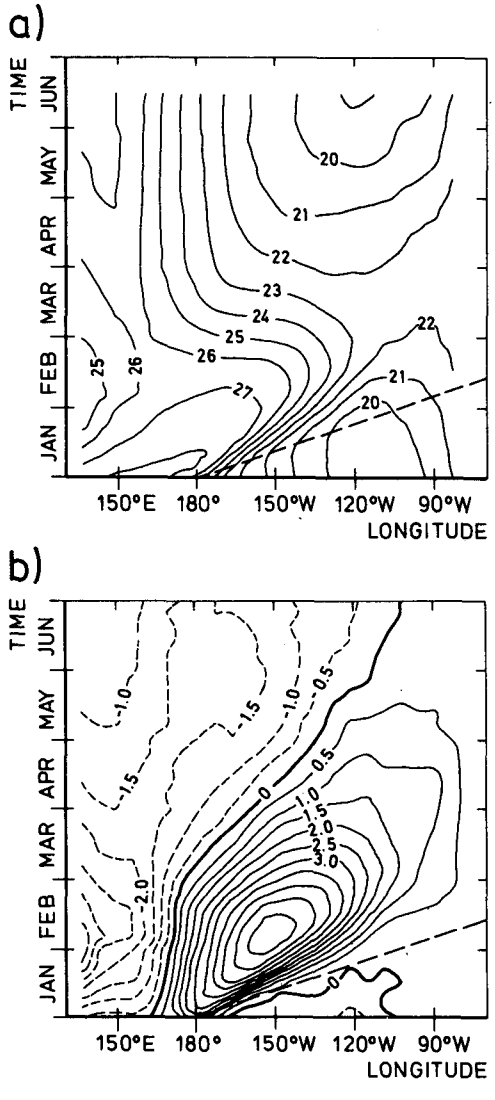

FIG. 7. As in Fig. 6, but for SST.

The evolution of SST in the uncoupled anomaly run is presented in Fig. 7a. Initially, there is an eastward surge of warm water due to the strong westerly wind stress anomaly. The first SST signal seems to propagate also with the speed of the first mode Kelvin wave, as can be seen from the SST anomaly chart (Fig. 7b). However, the subsequent warming is delayed compared to the rise in sea level (Fig. 6b). The delay increases as one goes eastward. The biggest SST anomaly at the eastern boundary appears in April, when sea level is already near normal. The anomalous warming is due to the contribution of zonal advection of temperature by anomalous surface currents (Fig. 8). Zonal current anomalies are strongest within the region of anomalous forcing, reaching values of a few meters per second in this region. The strength of anomalous currents decreases considerably further to the east. For this reason the tendency of SST anomalies is strongest in the central Pacific, where a strong mean SST gradient exists (Fig. 2a) and zonal currents are still strong, while SST changes are slowed down in the east. The zonally varying strength of zonal surface current leads therefore to the spreading of the isotherms, which is seen in Fig. 7b. In the central Pacific, in the vicinity of the dateline SST returns very quickly to normal conditions after the westerly winds have been turned off. The eastern Pacific is again much more inert with respect to SST changes.

In the very western part of the basin SST decreases by about 3°C. This result is due to the evolution of strong eastward currents along the equator (Fig. 8), which push the water away from the western boundary. This water is replaced by colder water from deeper levels, leading to the negative SST anomalies in the western Pacific.

c. *Coupled runs*

The coupled experiments were performed in the same way as the uncoupled runs. Initial conditions for the coupled model were taken from the uncoupled control runs, which were performed using observed seasonal forcing. The first experiment with the coupled model may be regarded as a reference run. In this experiment ("coupled control" run) the integration was continued after the coupling for 16 months. Because of the method of coupling using the flux correction technique, described above, the transition from the uncoupled control runs to the coupled control run is continuous. This can be seen in Fig. 9, which shows the SST along the equator as function of time before and after the coupling. No significant climate drift appears after the coupling. The coupled model undergoes essentially the same seasonal cycle, as expected because of the seasonally dependent flux correction. In general, the SST in the coupled control run shows more high frequency variability than in the uncoupled case, but indications of low frequency changes are not found.

The reaction of the coupled model to an externally introduced anomaly of surface wind stress is investigated in the next experiment ("coupled anomaly" run). As in the uncoupled anomaly run, we introduced a wind burst over the western Pacific. This wind burst has the same temporal and spatial characteristics as in the uncoupled case. This means that during the first month of the coupled anomaly run the wind stress is not calculated interactively over the western equatorial Pacific: although, the atmosphere model responds to the SST of the ocean model, the ocean model is exposed to the stress of the atmosphere model only outside of the region of anomalous forcing. After this first month the wind stress is fully interactive everywhere and the integration is continued for 11 further months. Anomalies of fields are calculated by subtracting the values of the coupled control run from the values of the coupled anomaly run.

In Figs. 10 and 11 we present the evolution of sea level and SST in the coupled anomaly run, and their anomalies with respect to the coupled control run, while Fig. 12 shows the zonal surface current anomalies. During the first month sea level, SST, and zonal currents in the coupled anomaly run show no significant differences relative to the uncoupled case (Figs. 6, 7 and 8). Kelvin waves propagate eastward and set up anomalous conditions in the ocean.

As soon as the atmosphere model is allowed to in-

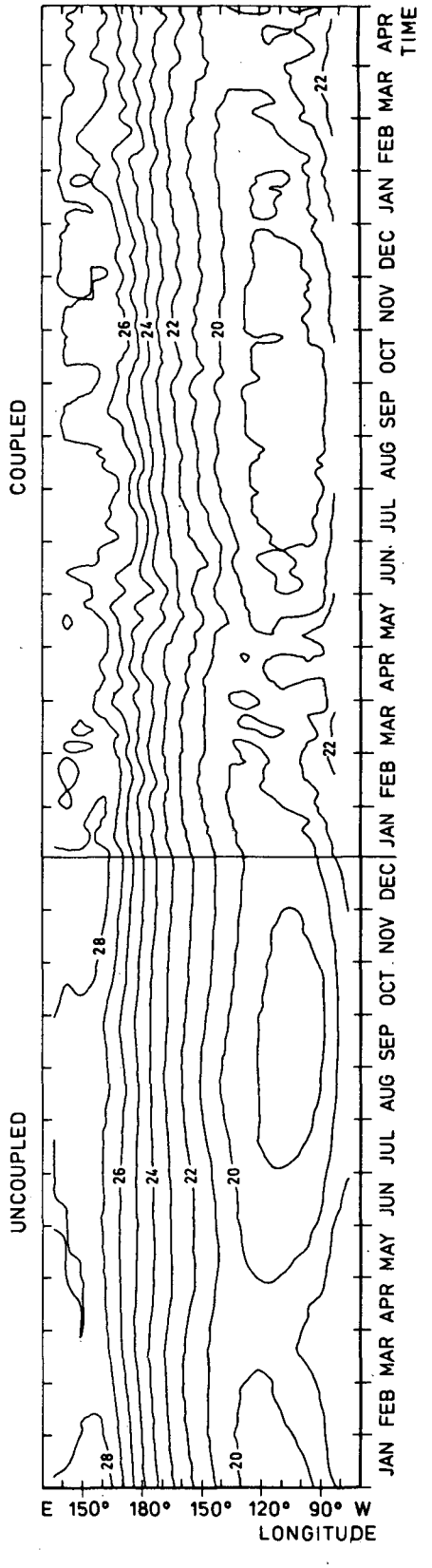

FIG. 9. Evolution of SST along the equator before and after coupling.

teract with the ocean model via wind stress over the entire ocean, differences in the oceanic response relative to the uncoupled run become obvious. Although the Hovmoeller diagram of sea level along the equator (Fig. 10a) still shows the propagation of a Kelvin wave after the wind anomaly has been turned off, the fall in sea level is not as strong as in the uncoupled case. After the passage of the Kelvin wave a positive sea level anomaly of the order of 10 cm is still present to the east of the dateline in the coupled case. The evolution of SST is also very different compared with the uncoupled case. While the isotherms at the dateline show already a westward tilt in February in the uncoupled run (Fig. 7a), the SST pattern in the coupled anomaly run is almost stationary at this time (Fig. 11a). The increase in the duration of anomalous conditions in the ocean may be attributed to the evolution of low level westerly winds in the atmosphere. As can be seen from Fig. 13, a regime of westerly wind stress, extending to the east of the dateline, has already been established in February. The westerly winds drive anomalous eastward surface currents (Fig. 12). Typical surface current anomalies are of the order 0.5 to 1 m s^{-1}.

The westerly winds undergo strong temporal variations, with episodes of weaker and with stronger westerlies of typical duration of the order of one week.

In the eastern Pacific we still find easterly surface winds of the same strength as the westerlies. Therefore a well defined convergence zone develops slightly to the east of the dateline. Together with the eastward shift of the warmest water (Fig. 11a), the anomalous convergence over the central Pacific leads to an eastward movement of the zone of heaviest convective rainfall (Fig. 14). At the end of February the strongest convective rainfall is located at a longitude of about 150°W. Like the wind stress, the rainfall pattern also shows evidence of temporal variations on the time scale of weeks. The simulated precipitation during episodes of strongest rainfall is of the order of 40 mm day^{-1}. The occurrence of low level westerly winds in the western Pacific and the shift of convective rain activity to the east indicates an eastward shift of the ascending branch of the Walker Circulation.

The first two months are followed by a period of slow changes. Sea level and SST fall to the east of the dateline (Figs. 10a and 11a), and the area of easterly winds expands westward (Fig. 13). Consequently, the region of heaviest convective rainfall also moves westward (Fig. 14). At the end of June, sea level anomalies have reduced to values of about 5 cm (Fig. 10b), while SST anomalies lie about two to three degrees above normal (Fig. 11b). Zonal surface current anomalies (Fig. 12) in the western and central Pacific are still eastward. Maximum rainfall is located to the east of the dateline at a longitude of 170°W at the end of June. From July to October sea level and SST do not show any significant changes. Westerly winds are still found in the western Pacific, but the strength of these westerlies is diminishing slightly until October (Fig. 13). The rainfall pattern continues to move westward.

In the second half of October, a strong westerly pulse appears in the zonal wind stress. As can be seen from Fig. 13, this pulse attains values in its center of more than 0.12 N m^{-2}. Apart from the initially introduced disturbance of 0.18 N m^{-2}, the wind stress pulse in October is the strongest westerly wind stress event that occurred during the entire 12 month integration. The ocean model clearly responds to this wind event. The evolution of sea level shows evidence of Kelvin wave propagation, as can be seen from the eastward tilt of the isohypses in Fig. 10a. The passage of the Kelvin wave is seen even better in the sea level anomaly diagram (Fig. 10b), which shows positive anomalies of 10 cm at the eastern boundary one month after the westerly winds occurred in the western Pacific. Along the path of the Kelvin wave the easterlies are anomalously weak (Fig. 13), which is favourable for its amplitude at the eastern boundary. The SST pattern (Fig. 11) shows also an eastward movement of the isotherms and SST anomalies increase up to 4°C in their center. Zonal surface currents exhibit strong eastward anomalies reaching values of 2 m s^{-1}. The region of most intense rainfall is also shifted slightly to the east with maximum values of the order of 40 mm day^{-1}.

The duration of the westerly wind stress pulse is about two weeks. After this pulse the area of westerlies decreases considerably. In December, easterlies are found along the equator only, except for the very eastern part (Fig. 13). In the central and eastern Pacific there is a strong tendency to a return to normal conditions. To the east of the dateline, anomalies of sea level and SST have almost disappeared at the end of December (Figs. 10a and 11a). In the western Pacific, however, sea level remains considerably below normal.

The horizontal structure of the coupled model's response to the initial wind burst is shown in Figs. 15, 16 and 17. SST anomalies develop rather quickly (Fig. 15). We find already an anomaly of about two degrees in the monthly mean chart for January (Fig. 15a). The SST anomalies then spread eastward and intensify until March. Thereafter the anomalies decrease slightly. Although the anomalies show large scale behavior, the eastern Pacific is almost unaffected. In the western Pacific we find over a considerable belt of latitudes negative anomalies. This dipole pattern of SST anomalies changes only slowly in space and time. In summary, the evolution of SST anomalies show basically the behaviour of a standing rather than a propagating mode.

Anomalous wind stress vectors (Fig. 16) within the equatorial belt evolve as one would expect from simple models (e.g., Gill, 1980). One finds an anomalous convergence over the center of the SST anomaly during all months beginning with February. The two inflow branches on the equator have different strength. Anomalous westerlies to the west of the maximum SST anomaly are stronger than the anomalous easterlies to

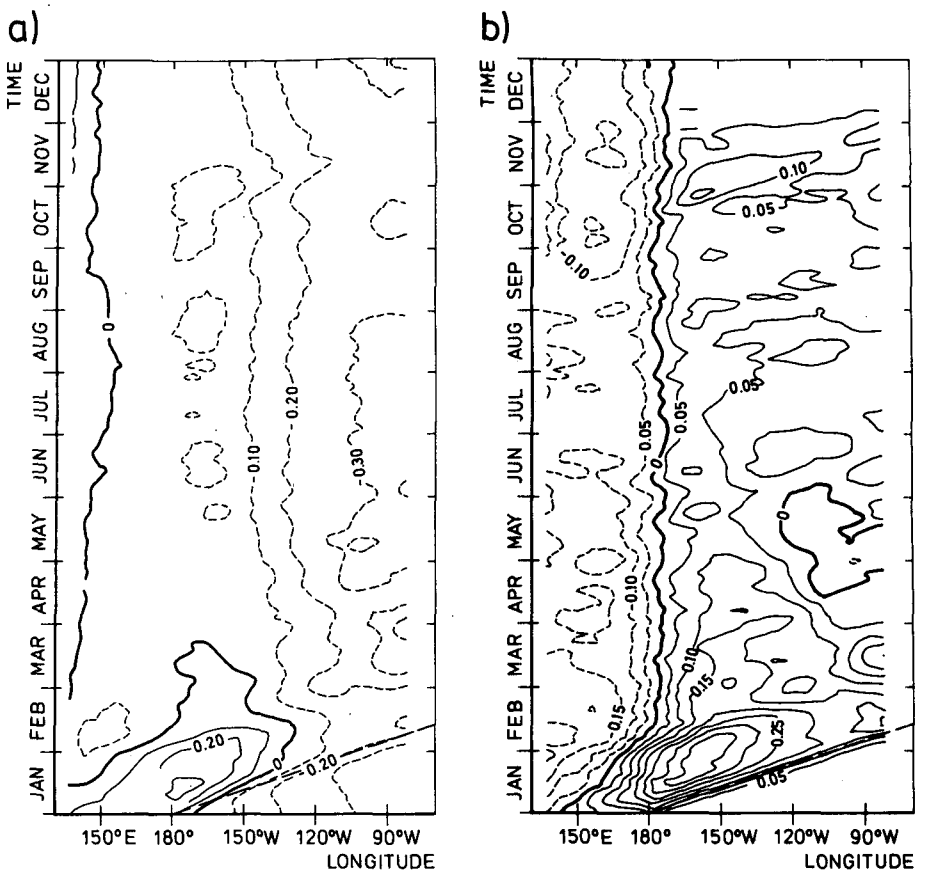

FIG. 10. Evolution of sea level along the equator for the coupled anomaly run, (a) full signal (contour interval 0.1 m) and (b) anomalies (contour interval 0.05 m).

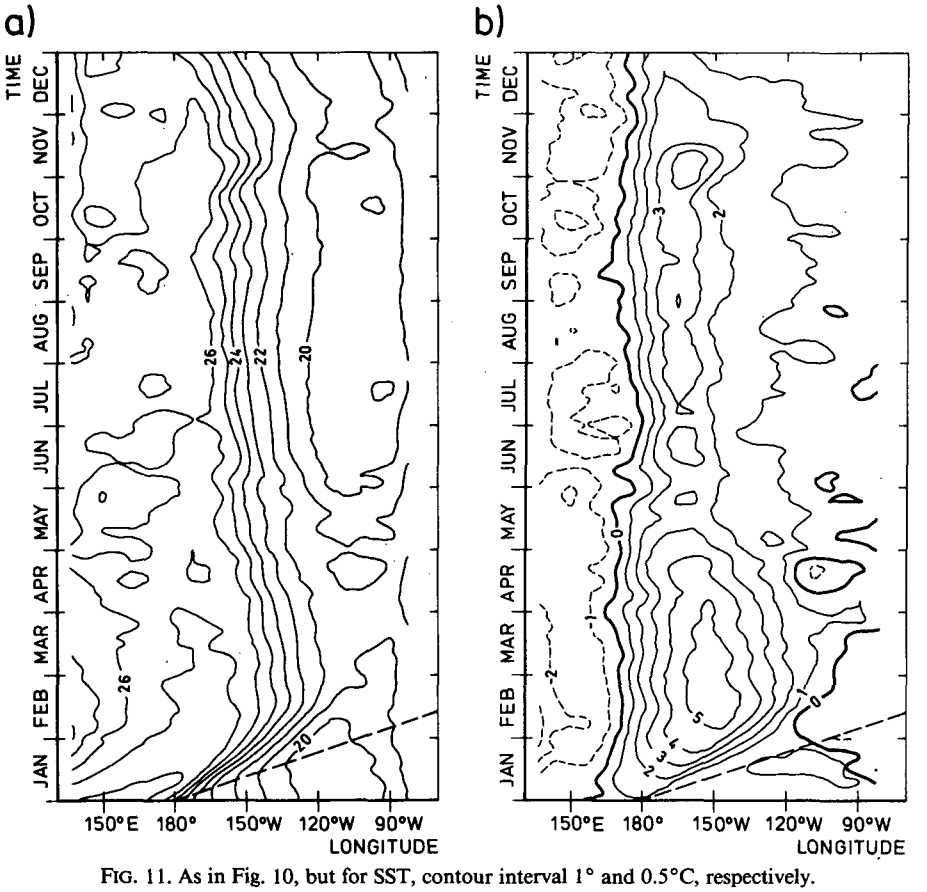

FIG. 11. As in Fig. 10, but for SST, contour interval 1° and 0.5°C, respectively.

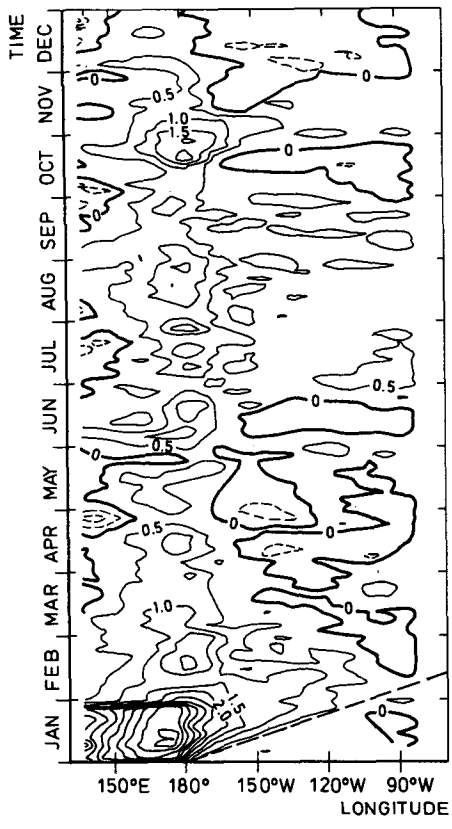

FIG. 12. Evolution of zonal surface current anomalies along the equator for the coupled anomaly run, contour interval 0.5 m s^{-1}.

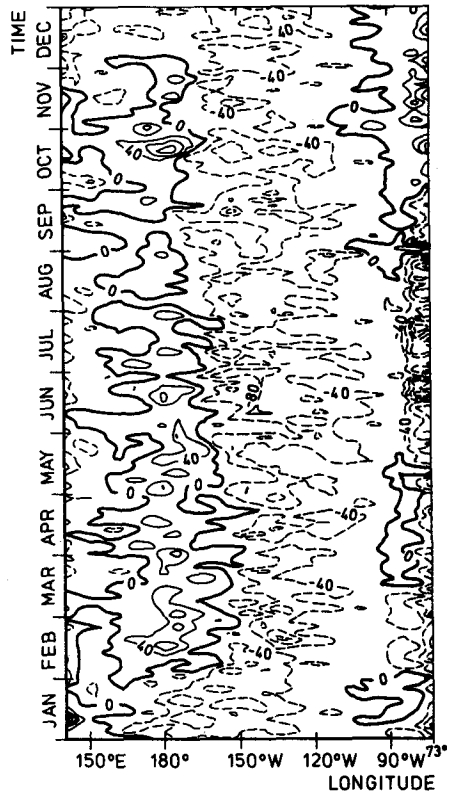

FIG. 13. Evolution of zonal wind stress along the equator for the coupled anomaly run, contour interval 40 mPa.

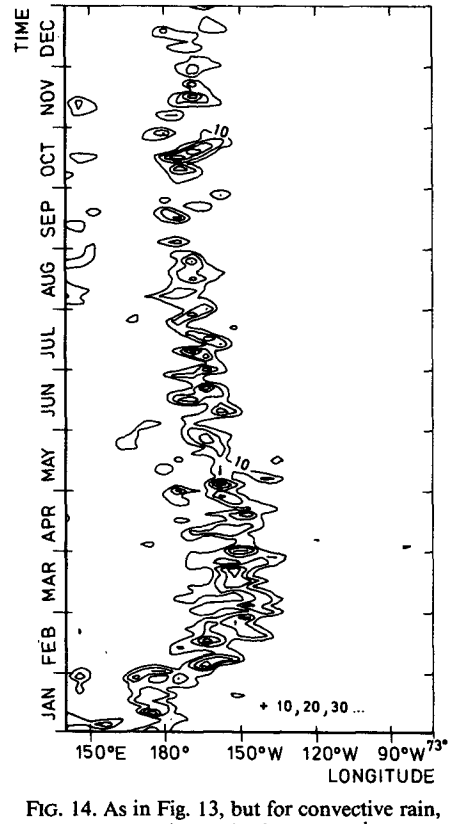

FIG. 14. As in Fig. 13, but for convective rain, contour interval: 10 mm day^{-1}.

the east of the SST anomaly, leading to a zonally asymmetric response.

A significant modification of the Walker Circulation is also indicated by the patterns of anomalous streamfunction (Fig. 17). In lower levels (Fig. 17a) one finds cyclones on either side of the equator, centered slightly to the east of the dateline. This leads to anomalous westerlies directly on the equator, as already discussed above (Fig. 15), resulting in a weakening of the lower branch of the Walker Circulation. The opposite response is found in upper levels, indicating a first mode baroclinic structure of the atmospheric response. At the 200 hPa level we find a pair of anticyclones around the equator. Between these two anticyclones the flow is westward, so that the strength of the normal eastward return flow of the Walker Circulation is reduced.

Over the eastern Pacific the streamfunction response is reversed compared to the central Pacific: at the 850 hPa level (Fig. 17a) one finds two anticyclones around the equator, while in the 200 hPa chart two cyclones occur at about 120°W (Fig. 17b). The different response patterns of the tropical streamfunction over the central and eastern Pacific suggest an excitation of a quadrupole pattern in the model. Such a quadrupole response was also found by Hoskins (personal communication) in a theoretical study.

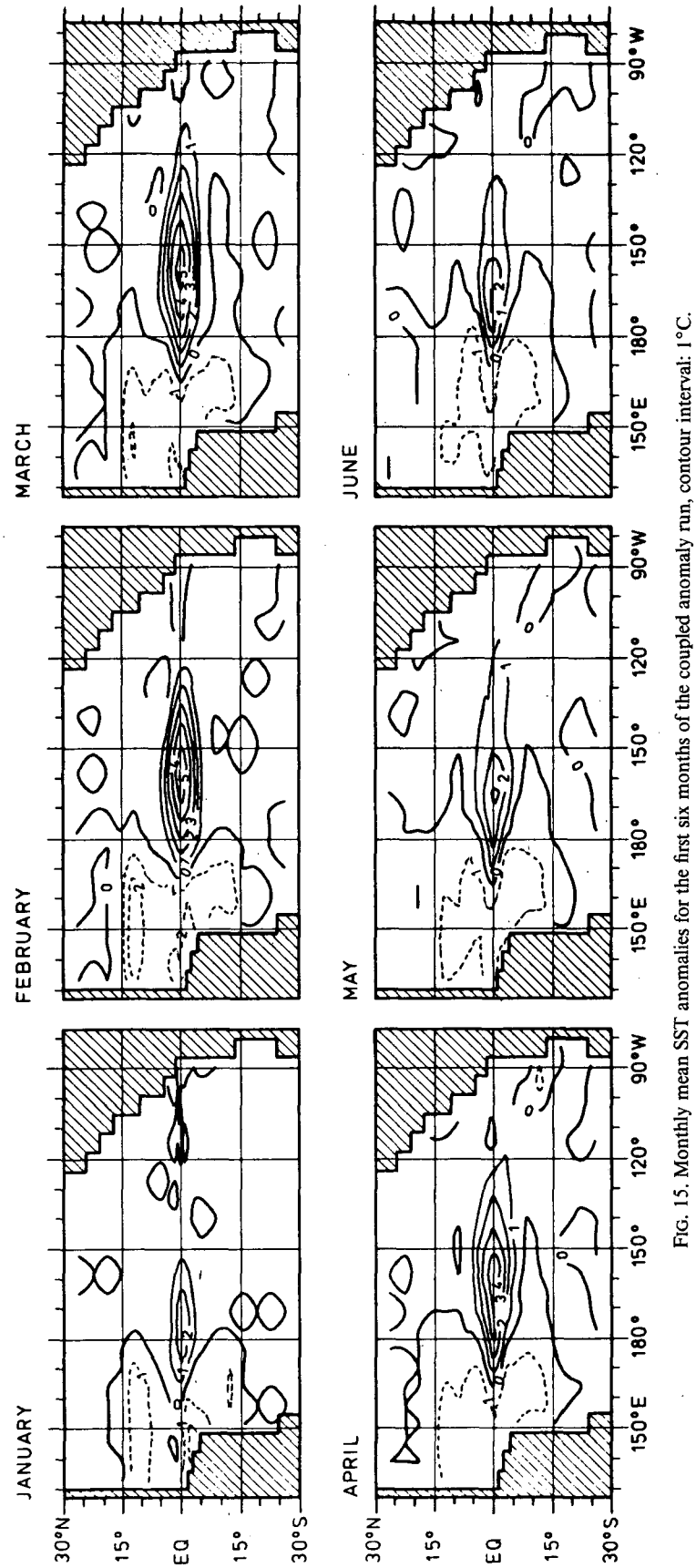

FIG. 15. Monthly mean SST anomalies for the first six months of the coupled anomaly run, contour interval: 1°C.

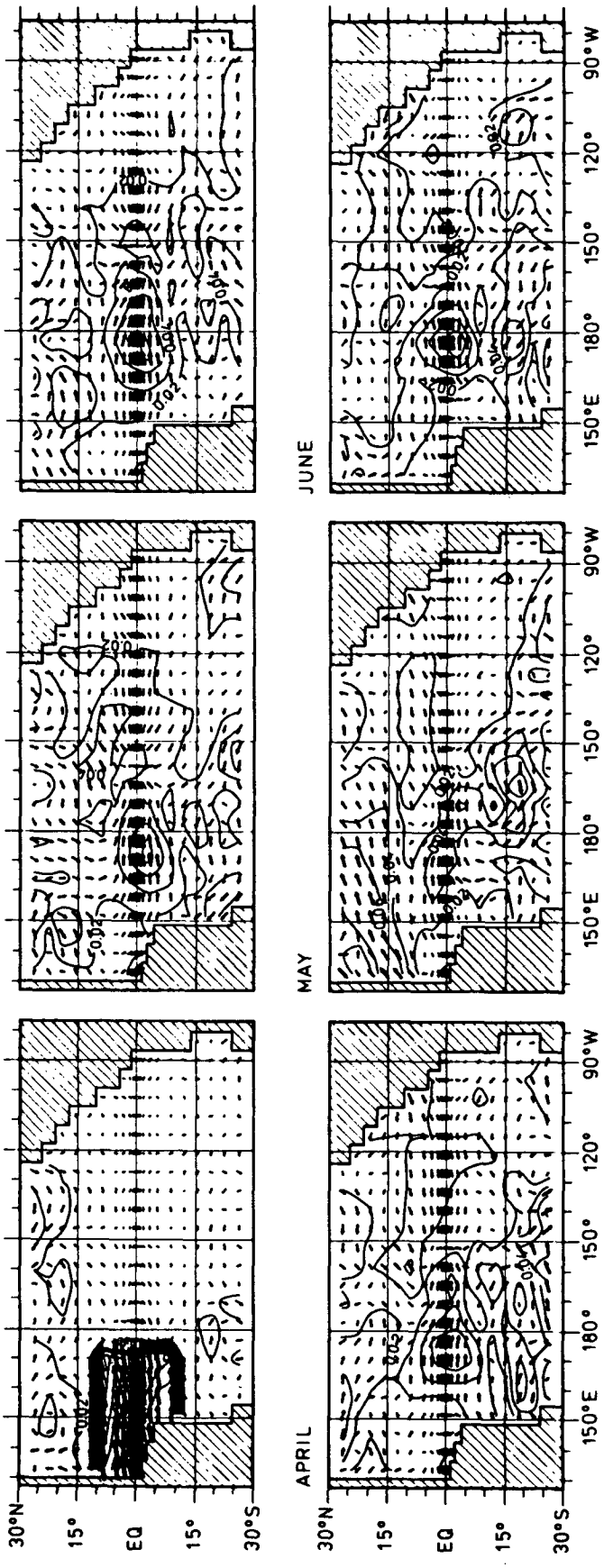

FIG. 16. As in Fig. 15, but for wind stress anomalies. Contours show the magnitude of the anomalies, contour interval: 0.02 N m^{-2}.

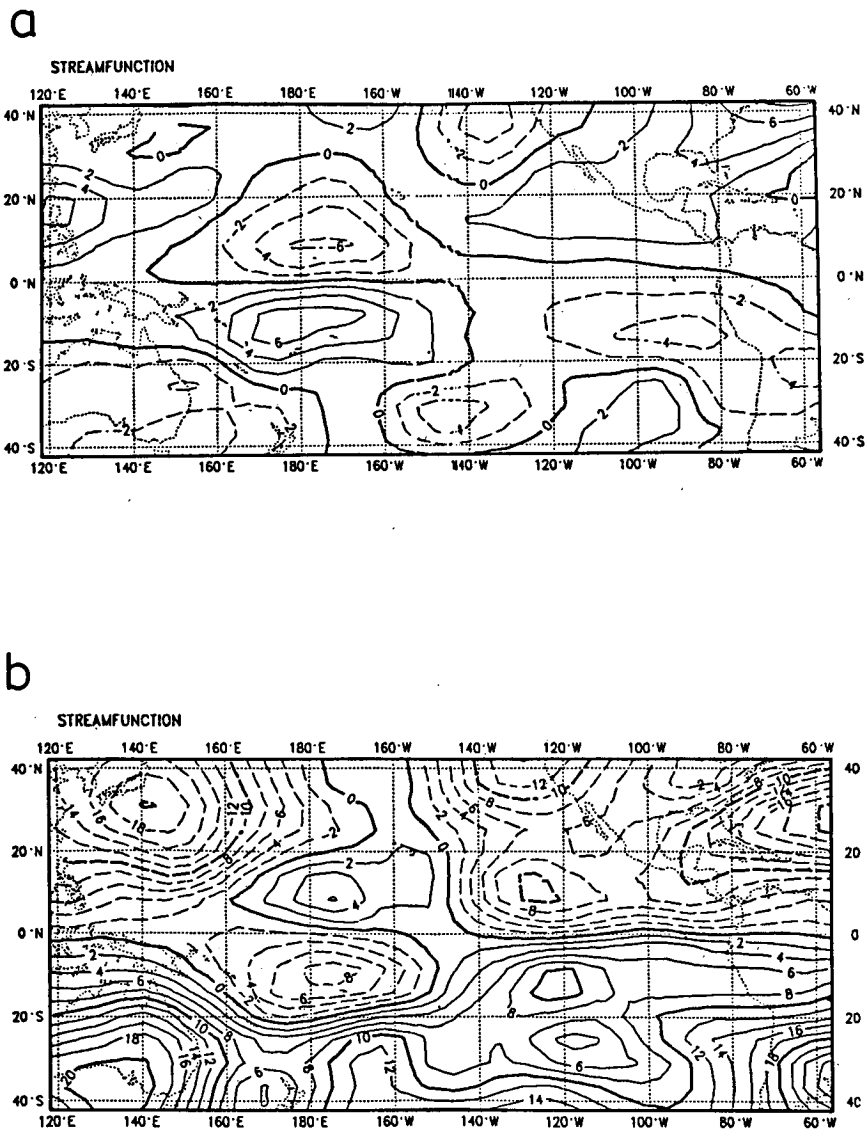

FIG. 17. Monthly mean streamfunction anomalies for February of the coupled anomaly run, (a) 850 hPa level and (b) 200 hPa level, contour interval: 2×10^{-6} m^2 s^{-1}.

The entire pattern of anomalous tropical streamfunction is very persistent and does not change significantly during the following months.

d. Dependence on date of initial burst

Several authors have pointed out the importance of the seasonal cycle for the ENSO phenomenon (e.g., Philander 1983; Cane 1986). The most prominent feature among the seasonal changes is the seasonal migration of the intertropical convergence zone (ITCZ): it is located at a latitude of about 10°N in August and September, while it has its most southern position at about 3°N in February and March. The southward movement of the ITCZ is associated with weak winds, which in turn favour warm conditions in the equatorial southeastern Pacific. For this reason it can be speculated that the evolution of ENSO events is dependent on the phase of the seasonal cycle. In order to test the validity of this hypothesis in our model, we repeated the burst experiment described above with initial conditions taken from another phase of the seasonal cycle. The coupled model is now initialized with July conditions taken from the uncoupled control runs. As in the former experiment, we introduced a westerly wind stress burst over the western Pacific. During July the wind stress over the western equatorial Pacific (see Fig. 1) is assumed to be purely zonal with a strength of 0.18 N m^{-2}, and the integration was then continued for the rest of the year.

In general, the response of the coupled model to the initial wind disturbance in this experiment is very similar to the response described in the previous subsection. Sea surface temperature along the equator (Fig. 18) evolves in the same manner as in the January experiment (Fig. 11a). The warmest water moves again from the western into the central Pacific during the first two months. This period of initial warming is then also followed by a period of slow changes.

The zonal wind stress component (Fig. 19) shows also basically the same behavior as in the January experiment (Fig. 13). Low level westerly winds over the western Pacific have developed after one month in response to the initial SST anomaly and maintain anomalous conditions after the artificial wind stress disturbance has been turned off in August. The situation remains almost unaltered until in the middle of November a strong westerly wind burst develops by internal dynamics. The location of this westerly wind stress pulse coincides roughly with that found in the January experiment (Fig. 13). As can be seen from Fig. 19, the zonal extent of the burst is only half of that which occurred during late October in the first experiment. However, the intensity of the wind stress burst is even stronger than in the former experiment. Its maximal values in the center are comparable to the value of the initially introduced artificial disturbance. In response to the westerly wind pulse, SST increases to the east of the dateline (Fig. 18). The warming stops rapidly after the westerlies have collapsed. During December, the westerlies are not well pronounced and a moderate cooling starts. Since the evolution of anomalous conditions was very similar to that found in the January experiment, the integration was stopped after six months.

The insensitivity of the model results to the date of the initial wind burst can be attributed to the bad representation of the ITCZ within the atmosphere model.

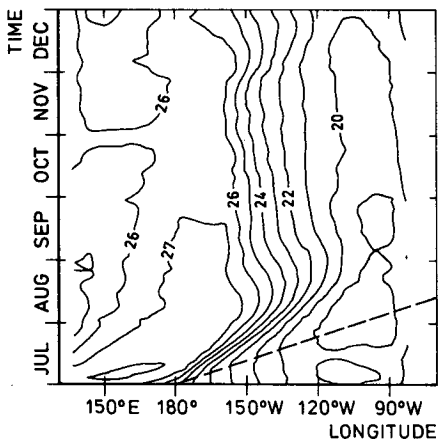

FIG. 18. As in Fig. 11, but from the experiment where the wind burst was introduced in July.

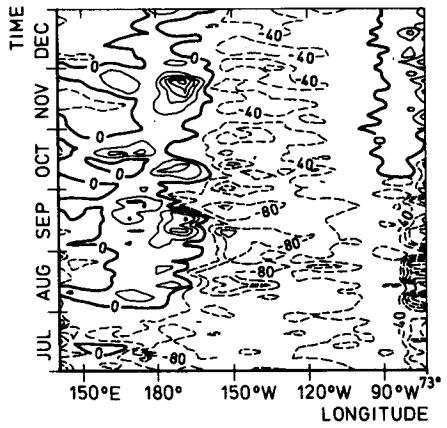

FIG. 19. As in Fig. 13, but from the experiment where the wind burst was introduced in July.

The strength of the ITCZ is severely underestimated by the atmosphere model (Fig. 4a), and it does not simulate the observed migration of the ITCZ. The inability of the atmosphere model in simulating a realistic ITCZ and its seasonal migration may be attributed to the rather coarse resolution, which is equivalent to a 5.6×5.6 grid. With such a low horizontal resolution the model can neither resolve a narrow and strong ITCZ nor its seasonal migration.

4. Summary and discussion

A coupled ocean–atmosphere general circulation model has been developed for ENSO related problems. Both components of the coupled system have already been tested with respect to boundary forced low frequency variability and were successful in reproducing observed variations of typical circulation indices (Latif, 1987; Kirk, personal communication). In this study, the two models interact via sea surface temperature and surface wind stress. The heat flux into the atmosphere is computed using the ocean model's SST, but the heat flux into the ocean is not taken from the atmosphere model, but is determined diagnostically from the observed air temperature at 2 m height. We make use of a flux correction technique to avoid a climate drift of the coupled system.

In a pilot study we investigated the response of the coupled model to an initially introduced disturbance of surface wind stress. The results are compared with the results of the ocean model, run in an uncoupled mode, and with that of the coupled model, run without initial disturbance. With the coupled model, anomalous conditions in the ocean are much more persistent than in the uncoupled case. The increase in persistence is due to the feedback by the atmosphere. It is shown that an eastward shift of the ascending branch of the Walker Circulation is responsible for the increase in persistence. This eastward shift is accompanied by

westerly surface winds in the western Pacific (Fig. 13) and by a displacement of the convective rainfall zone, which is usually located over the far western Pacific. After these anomalous conditions have been established within the first two months, the situation changes only very slowly. The coupled system shows evidence of the excitation of an unstable standing mode, which appears to be independent of the season.

One basic objective of the present study was to test the coupled model with respect to the performance of an externally excited ENSO event. Although the coupled model shows evidence of an unstable mode, the evolution of anomalous conditions is nevertheless inconsistent with the observations in some important points. The pattern of SST (Fig. 11a), for instance, does not evolve in the usual manner. As was shown by Gill (1983), during ENSO events one observes a significant weakening of the equatorial cold water tongue. In our model simulation we find no such a weakening. The east–west contrast of SST remains almost unaltered, and the coupled model shows only an eastward shift of the region of strongest zonal SST gradient. Furthermore, because of the coastal upwelling at the western boundary in response to intense eastward surface currents (Fig. 12), the western Pacific tends to cool. Thus, the warmest water is located in the central Pacific, whereas the observations indicate an expansion of the warmest water to the east and an almost uniform SST in the western and central Pacific (e.g., Fu et al., 1986).

Another unrealistic feature in the response of the coupled model is the lack of any significant propagation of the anomalies, especially of SST and surface wind stress. Gill and Rasmusson (1983) demonstrated that during the 1982/83 ENSO event the anomalous conditions in both the atmosphere and the ocean propagated eastward. The estimated speed was about 1 m s^{-1}. As shown by Kirk (personal communication) and Latif (1987), both the ocean and atmosphere model, when run in an uncoupled mode with observed boundary values as forcing, show such a propagation for this particular event. The propagation in this case is therefore presumably due to the propagation of the forcing fields rather than internal processes within the models.

We suggest three possible reasons for the lack of these important features of ENSO events in our model simulation. First, the ocean model may be too inert through the choice of constant vertical mixing coefficients. In particular, the current variability appears to be weaker than observed. Additional experiments are therefore planned with non-constant coefficients, as suggested by Pacanowski and Philander (1981).

The second reason may lie in the atmosphere model. As is shown by Kirk (personal communication), the tropical response of the atmosphere model to realistic SST anomalies is weaker than the observed response. For example, anomalies of surface wind stress within the simulation of the 1982/83 ENSO event are approximately halved compared with the FSU dataset (Goldenberg and O'Brien, 1981).

Finally, the flux correction method of removing model drift may inadequately compensate all systematic deficiencies if strong nonlinearities are involved.

At the present stage we cannot decide which of these reasons are responsible for the shortcomings of the model simulation. Further analysis of the model results is therefore needed, as well as more experiments using different parameterizations and coupling techniques.

Although the simulated evolution of SST misses some important aspects of ENSO events, the large scale equatorial warming is clearly reproduced (Fig. 15). The atmosphere model responds to this large scale warming with an anomalous circulation, which is associated with an eastward shift of the Walker Circulation. The atmospheric response is consistent with several observed features, such as the zonally asymmetric response of low level winds (Fig. 16), the eastward shift of the region of heaviest rainfall (Fig. 14), and the first-mode baroclinic nature of the tropical streamfunction pattern (Fig. 17).

An interesting feature is the occurrence of intense westerly wind bursts over the western Pacific in the anomaly runs (Figs. 13 and 19), which developed by internal dynamics. Such bursts are known to occur from time to time over the western equatorial Pacific. In the coupled control run performed without initial disturbance, however, these bursts over the western Pacific were not found. We suggest an explanation of this difference with the aid of the 30–60 day Oscillations. It has been speculated by various authors (e.g., Lau and Lau, 1986) that the occurrence of the 30–60 day Oscillations is due to instabilities within the Indonesian convective zone. As shown in Bruns et al. (1987), the atmosphere model contains these oscillations, but the amplitudes of these waves are underestimated in the model. If the assumption is correct that the 30–60 day waves are excited by convection, the region of the 30–60 wave activity should move eastward as the convection zone shifts eastward (Fig. 14). As the 30–60 day waves propagate eastward, they should be able to move from the Indonesian area into the western Pacific and thereby affect the Pacific Ocean also under the normal conditions of the coupled control run. It is possible that the lack of any wind bursts over the western Pacific in the coupled control run is a result of a too strong damping of the 30–60 day waves in the atmosphere model as they propagate eastward, as suggested by their weak amplitude.

In further studies we intend to investigate the importance of a fully interactive surface heat flux. For this purpose a repeat of above described experiment is planned with a fully interactive heat flux included. The coupled model will then also be run for a period of the order of ten years in order to determine the full variability spectrum of the coupled model.

Acknowledgments. The authors appreciate very much the assistance of U. Schlese and the staff of the "Meteorologisches Institut" at the University of Hamburg in advising us in using the atmosphere model. Many thanks also to Dr. E. Maier-Reimer for helpful discussions and to Mrs. M. Grunert for preparing the figures.

REFERENCES

Biercamp, J., and H. von Storch, 1987: Exchange of energy and momentum at the oceans surface. Climate simulations with the ECMWF T21 model in Hamburg, Large scale atmospheric modelling, Rep. No. 1, G. Fischer Ed., Meteorologisches Institut der Universitaet, Bundesstr. 55, D 2000 Hamburg 13, F.R.G.

Bruns, T., I. Fischer-Bruns and H. von Storch, 1987: The structure and propagation of seasonal and intraseasonsl oscillations in the tropical T 21 atmosphere model. Climate simulations with the ECMWF T21 model in Hamburg, Large scale atmospheric modelling, Rep. No. 1, G. Fischer Ed., Meteorologisches Institut der Universitaet, Bundesstr. 55, D 2000 Hamburg 13, F.R.G.

Bryan, K., and S. Manabe, 1985: A coupled ocean–atmosphere and the response to increasing CO_2. *Coupled Ocean-Atmosphere Models.* J. C. J. Nihoul, Ed., Elsevier Oceanogr. Ser. Vol. 40.

Cane, M. A., 1983: Oceanographic events during El Niño. *Science,* **222,** 1189–1195.

——, 1986: El Niño. *Ann. Rev. Earth Planet. Sci.,* **14,** 43–70.

——, S. E. Zebiak and S. C. Dolan, 1986: Experimental forecasts of El Niño. *Nature,* **231,** 810–811.

Duemenil, L., and U. Schlese, 1987: Description of the general circulation model. Climate simulations with the ECMWF T21 model in Hamburg, Large scale atmospheric modelling, Rep. No. 1, G. Fischer Ed., Meteorologisches Institut der Universitaet, Bundesstr. 55, D 2000 Hamburg 13, F.R.G.

Esbensen, S. K., and Y. Kushnir, 1981: The heat budget of the global ocean: an atlas based on estimates from surface marine observations. Climate Research Institute, Rep. No. 29, Oregon State University, Corvallis, Oregon, U.S.A.

Fennessy, M. J., L. Marx and J. Shukla, 1985: General circulation model sensitivity to 1982–83 equatorial sea surface temperature anomalies. *Mon. Wea. Rev.,* **113,** 858–864.

Fu, C., H. F. Diaz and J. O. Fletcher, 1986: Characteristics of the response of sea surface temperature in the central Pacific associated with warm episodes of the Southern Oscillation. *Mon. Wea. Rev.,* **114,** 1716–1738.

Gates, W. L., Y. J. Han and M. E. Schlesinger, 1985: The global climate simulated by a coupled atmosphere-ocean general circulation model: preliminary results. *Coupled Ocean–Atmosphere Models,* J. C. J. Nihoul, Ed., Elsevier Oceanogr. Ser. Vol. 40.

Gill, A. E., 1980: Some simple solutions for heat-induced tropical circulation. *Quart. J. Roy. Met. Soc.,* **106,** 447–462.

——, 1983: An estimation of sea level and surface current anomalies during the 1972 El Niño and consequent thermal effects. *J. Phys. Oceanogr.,* **13,** 586–606.

——, and E. M. Rasmusson, 1983: The 1983–83 climate anomaly in the equatorial Pacific. *Nature,* **306,** 229–234.

Goldenberg, S. O., and J. J. O'Brien, 1981: Time and space variability of tropical Pacific wind stress. *Mon. Wea. Rev.,* **109,** 1190–1207.

Haney, R. L., 1971: Surface thermal boundary condition for ocean circulation models. *J. Phys. Oceanogr.,* **1,** 241–248.

Hirst, A. C., 1985: Free equatorial instabilities in simple coupled atmosphere–ocean models. *Coupled Ocean–Atmosphere Models.* J. C. J. Nihoul, Ed., Elsevier Oceanogr. Ser., Vol. 40.

Kirk, E., M. Ponater and A. Kirk, 1987: Circulation statistics of the T21 GCM. Climate simulations with the ECMWF T21 model in Hamburg, Large scale atmospheric modelling, Rep. No. 1, G. Fischer Ed., Meteorologisches Institut der Universitaet, Bundesstr. 55, D 2000 Hamburg 13, F.R.G.

Latif, M., 1987: Tropical ocean circulation experiments. *J. Phys. Oceanogr.,* **17,** 246–263.

Lau, K. M., 1985: Elements of a stochastic dynamical theory of the long-term variability of the El Niño/Southern Oscillation. *J. Atmos. Sci.,* **42,** 1552–1558.

Lau, N. C., 1985: Modeling the seasonal dependence of the atmospheric response to observed El Niños in 1962–76. *Mon. Wea. Rev.,* **113,** 1970–1996.

——, and K. M. Lau, 1986: The structure and propagation of intraseasonal oscillations appearing in a GFDL GCM. *J. Atmos. Sci.,* **43,** in press.

McCreary, J., 1976: Eastern tropical response to changing wind systems: with application to El Niño. *J. Phys. Oceanogr.,* **6,** 632–645.

Pacanowski, R. C., and S. G. H. Philander, 1981: Parameterization of vertical mixing in numerical models of tropical oceans. *J. Phys. Oceanogr.,* **11,** 1143–1451.

Philander, S. G. H., 1983: El Niño–Southern Oscillation phenomena. *Nature,* **302,** 295–301.

——, 1986: Predictability of El Niño. *Nature,* **321,** 810–811.

——, T. Yamagata and R. C. Pacanowski, 1984: Unstable air–sea interactions in the tropics. *J. Atmos. Sci.,* **41,** 604–613.

——, and A. D. Seigel, 1985: Simulation of El Niño of 1982–1983. *Coupled ocean–atmosphere models.* J. C. J. Nihoul, Ed., Elsevier Oceanogr. Ser. Vol. 40.

Rasmusson, E. M., and J. M. Wallace, 1983: Meteorological aspects of the El Niño/Southern Oscillation. *Science,* **222,** 1195–1202.

Sausen, R., K. Barthel and K. Hasselmann, 1987: Coupled ocean-atmosphere models with flux correction. Max-Planck-Institut fuer Meteorologie, Rep. No. 1, Bundesstr. 55, D 2000 Hamburg 13, F.R.G.

Schopf, P., and M. Suarez, 1987: Vacillations in a coupled ocean–atmosphere model. *J. Atmos. Sci.,* in press.

Washington, W. M., A. J. Semtner, G. A. Meehl, D. J. Knight and T. A. Mayer, 1980: A general circulation experiment with a coupled atmosphere, ocean, and sea ice model. *J. Phys. Oceanogr.,* **10,** 1887–1908.

Wyrtki, K., 1985: Water displacements in the Pacific and the genesis of El Niño cycles. *J. Geophys. Res.,* **90,** 7129–7132.

Zebiak, S. E., 1984: Tropical atmosphere ocean interaction and the El Niño/Southern Oscillation phenomenon. Ph.D. thesis, Massachusetts Institute of Technology.